Toward atomic-resolution quantum measurements with coherently shaped free electrons

Supplementary Material

Ron Ruimy[†1], Alexey Gorlach[†1], Chen Mechel[1], Nicholas Rivera[2], and Ido Kaminer[1]

[1] *Solid State Institute, Technion-Israel Institute of Technology, Haifa 32000, Israel*
[2] *Department of Physics, Massachusetts Institute of Technology, Cambridge, MA, 02139, United States*

kaminer@technion.ac.il; † equal contributors

Section I – Validity of the two-level system model

In our research, we are interested in the possibility of using free electrons as a probe for quantum coherence in qubit systems. The measurements are made through electron energy loss spectroscopy (EELS), and we model the interaction as an interaction between the evanescent electric field of the free electron and the dipole moment of the two-level system (TLS). This model predicts that the electron can gain/lose a single quantum of energy while de-exciting/exciting the quantum TLS. In reality, the modeling of an emitter as a TLS frequently does not yield a good description, as a free electron beam scattering from atomic electrons can lose energy through a wide variety of phenomena. While an electron can excite a particular transition of interest through the mechanism outlined above, an electron can excite many additional transitions (such as core-shell transitions). Beyond the atom undergoing many types of transitions, the electron can also lose energy by many different channels besides a collision with the emitter of interest. The electron can lose energy via Bremsstrahlung processes, as well as via collective excitations (photons, phonons, and plasmons).

All these inelastic processes occur at a probability considerably smaller than unity for thin samples. The majority of the probability remains in electrons that do not undergo inelastic processes, also called the zero-loss peak (ZLP) in EELS. We are interested in EELS peaks that are related to a particular transition in the system (the "qubit" or "TLS" transition). We consider energy loss associated with other peaks in the EELS spectrum to be that of decoherence channels. Thus, in practice, whenever we measure an electron (after it passes through the sample) as having an energy that differs from E_0 or $E_0 \pm \hbar\omega_0$, we ignore it. We consider only materials for which the qubit transition is separated in energy from the other inelastic processes.

One concern is that different EELS peaks are not necessarily well-separated, especially if some are broad (such as the peaks associated with plasmons). These broad peaks may overlap the peak fitting the TLS transition. This problem is partially solved by using electrons in a superposition of two (or more) energy states, all spaced by $\hbar\omega_0$. In this case, we measure not the height of the peaks related to the TLS transition but the height difference between the two ZLPs (corresponding to the two initial energies of the electron) as they interfere with each other while interacting with the TLS. This interference between two initial energies relies on the coherence of the qubit and can significantly enhance the contrast in the measurements, as analyzed in the paper. Competing excitations, such as those of plasmon and phonon polaritons, have a very short coherence lifetime and therefore will not lead to the resulting interference between the two electron energies, i.e., will result in a relatively small change in the EELS spectra. Thus, we can neglect the decoherence channels, if the energy difference between the two ZLPs matches the qubit energy and assuming that the probabilities of the decoherence channels are considerably smaller than unity (not necessarily considerably smaller than the original spontaneous qubit transition). This idea is illustrated in Fig. 1.

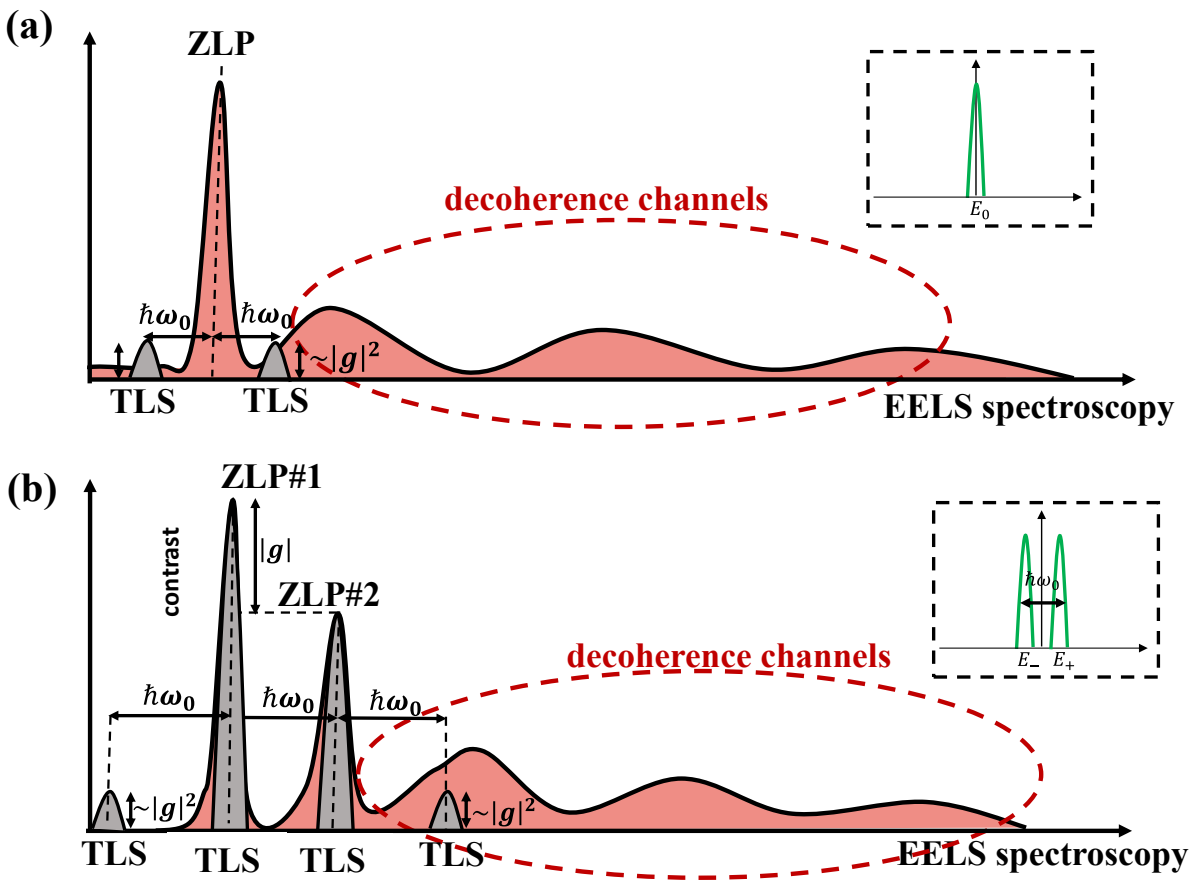

Fig 1. Schematic electron energy-loss spectrum (EELS) that highlights the electron transitions that can be controlled by coherently shaped free electrons. **(a)** The spectrum of an unshaped electron (electron wavefunction with Gaussian distribution of energy): the peak of the two-level system (TLS) excitation scales like $|g|^2$ and can frequently be considerably smaller than that of the other processes, which we call "decoherence channels." **(b)** The electron is shaped to have two different energies that can be thought of as two different zero-loss peaks (ZLPs). Their relative phase before the interaction creates a contrast in their height after the interaction that contains information about the state of the qubit. The contrast scales like $|g|$ if the qubit is in a coherent superposition state. The key to this enhancement is the interference of the shaped electron. Other contributions to the spectrum (here noted as decoherence channels), such as surface plasmon losses or peaks due to core-loss transitions [1], can be neglected when their probability is sufficiently small that they do not significantly alter the ZLP(s).

Section II – The quantum theory for the interaction of a free electron and a TLS

In this section, we discuss the interaction of a free electron with a quantum TLS through the dipole interaction in a fully quantum mechanical manner. We develop the 1D Hamiltonian that was used to obtain the results in the main text. This 1D Hamiltonian is based on the paraxial approximation for the electron, which is justified in the limit where the initial energy of the electron is considerably greater than that of the TLS.

The Hamiltonian consists of the free electron Hamiltonian (H_e), the TLS Hamiltonian (H_{TLS}), and the interaction Hamiltonian (V):

$$H = H_0 + V = H_{\mathrm{e}} + H_{\mathrm{TLS}} + V. \tag{1}$$

For a TLS with an energy gap of $\hbar\omega_0$, the Hamiltonian is represented by the Pauli matrix σ_z so that $H_{TLS} = \frac{\hbar\omega_0}{2}\sigma_z$ with $\sigma_z = |\mathrm{e}\rangle\langle\mathrm{e}| - |\mathrm{g}\rangle\langle\mathrm{g}|$, where e is the excited state and g the ground state. The interaction part of the Hamiltonian couples the TLS dipole moment to the electric field associated with a moving point charge (electron) $V = -\boldsymbol{d}\cdot\boldsymbol{E}$. This interaction term is justified under the dipole approximation in which we assume that the bound electron wavefunction is tightly confined to the atomic nuclei. The transition dipole operator is defined as

$$\boldsymbol{d} = \langle\mathrm{e}|e\boldsymbol{r}|\mathrm{g}\rangle\cdot|\mathrm{e}\rangle\langle\mathrm{g}| + \langle\mathrm{g}|e\boldsymbol{r}|\mathrm{e}\rangle\cdot|\mathrm{g}\rangle\langle\mathrm{e}| = \left(\boldsymbol{d}_{eg}\sigma_+ + \boldsymbol{d}_{eg}^*\sigma_-\right), \tag{2}$$

where $\boldsymbol{d}_{eg} = d_x\hat{\boldsymbol{x}} + d_y\hat{\boldsymbol{y}} + d_z\hat{\boldsymbol{z}}$. In this notation, we assume that the transition dipole operator is purely off-diagonal, which typically occurs as a result of the inversion symmetry of atoms. For a relativistic (spin-less) electron, the free electron Hamiltonian was given by Klein and Gordon [2],

$$H_e = c\sqrt{m^2c^2 + \boldsymbol{p}^2}\,. \tag{3}$$

We now simplify the Klein–Gordon Hamiltonian under the case in which we treat the electron under the paraxial approximation, which results from linearizing the dispersion relation of the electron around its central momentum. Stated more rigorously, we restrict the electron Hamiltonian to the space of functions of the form $\psi = e^{i\boldsymbol{k_0}\cdot\boldsymbol{r}}f$, where f is slowly varying ($|\nabla f| \ll |kf|$). In that case, the action of the electron Hamiltonian on the state is

$$H_e\psi = c\sqrt{m^2c^2 - \hbar^2\nabla^2}e^{i\boldsymbol{k_0}\cdot\boldsymbol{r}}f \approx e^{i\boldsymbol{k_0}\cdot\boldsymbol{r}}c\sqrt{m^2c^2 + \hbar^2\boldsymbol{k_0}^2 - 2i\hbar^2\boldsymbol{k_0}\cdot\nabla f}. \tag{4}$$

Taylor expanding and noting that in relativity $\frac{p}{E} = \frac{v}{c^2}$, we have

$$e^{i\overrightarrow{k_0}\cdot\vec{r}}\left(c\sqrt{m^2c^2 + \hbar^2\boldsymbol{k_0}^2} + \frac{\hbar c\boldsymbol{k_0}\cdot(-i\hbar\nabla)}{\sqrt{m^2c^2 + \hbar^2\boldsymbol{k_0}^2}}\right)f = e^{i\boldsymbol{k_0}\cdot\boldsymbol{r}}(E_0 - i\hbar\boldsymbol{v}\cdot\nabla)f. \tag{5}$$

We can replace the Hamiltonian with $H_e = -i\hbar\boldsymbol{v}\cdot\nabla$, as they are the same in this space of states up to the identity. Physically, this approximation states that, regardless of the electron's momentum, its velocity is v, which is a type of "no-recoil approximation." We assume that the electron is moving on the z-axis and that the TLS is located at $(0,0,0)$. We can then write the Hamiltonian as

$$H = -i\hbar v\partial_z + \frac{\hbar\omega_0}{2}\sigma_z + \left(\boldsymbol{d}_{eg}\sigma_+ + \boldsymbol{d}_{eg}^*\sigma_-\right)\cdot\boldsymbol{E}(r_\perp, 0, z), \tag{6}$$

where $\boldsymbol{E}(r_\perp, 0, z)$ is the electric field at the location of the TLS $(0,0,0)$ as a function of the electron's position $(r_\perp, 0, z)$ as given by the Maxwell equations. The motion of the electron and the position of the TLS are shown in Fig. 2

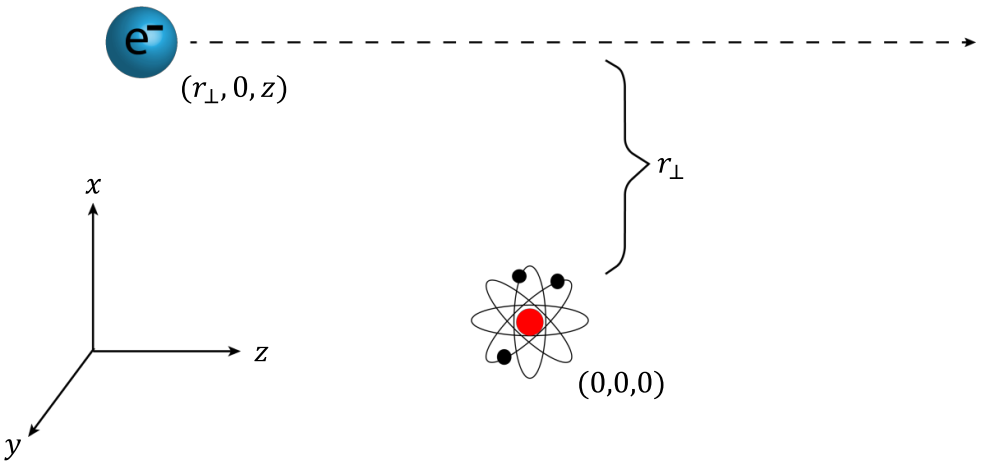

Fig. 2. Schematic of the interaction between a free electron and an atom. The electron has coordinates $x = r_\perp,\ y = 0$ and moves along the z-axis with speed v so that $z = vt$. The atom is taken as stationary and situated at the origin $(0,0,0)$.

Section III – Derivation of the scattering matrix and analysis of the interaction strength

In this section, we find an approximate solution to the scattering matrix resulting from the Hamiltonian in Eq. (6) through the Magnus expansion. We discuss the structure of the complete scattering matrix and show that an approximate form of it is highly accurate under the most realistic conditions in electron–TLS interactions. To solve the problem, it is convenient to move into the interaction picture in which

$$V_I(t) = e^{i\frac{H_0}{\hbar}t} V e^{-i\frac{H_0}{\hbar}t}, \tag{7}$$

where $H_0 = H_e + H_{TLS}$. Using the identity, $e^{vt\partial_z} f(z) e^{-vt\partial_z} = f(z + vt)$, we find

$$V_I(t) = \left(\boldsymbol{d}\sigma_+ e^{i\omega_0 t} + \boldsymbol{d}^*\sigma_- e^{-i\omega_0 t}\right) \cdot \boldsymbol{E}(r_\perp, 0, z + vt). \tag{8}$$

The S-matrix, $S = Te^{-\frac{i}{\hbar}\int_{-\infty}^{\infty} V_I(t)dt}$ (with T the usual time-ordering operator) can now be evaluated according to the Magnus expansion [3]:

$$S = Te^{-\frac{i}{\hbar}\int_{-\infty}^{\infty} V_I(t)\,dt} = e^{\sum_{k=1}^{\infty}\Omega_k(\infty)}, \tag{9}$$

where the Magnus expansion operators Ω_k are given by nested commutators of V_I at different times. For example, the first two terms of the expansion are given as

$$\begin{cases} \Omega_1(\infty) = -\dfrac{i}{\hbar}\displaystyle\int_{-\infty}^{\infty} dt\, V_I(t), \\ \Omega_2(\infty) = \dfrac{1}{2}\left(-\dfrac{i}{\hbar}\right)^2 \displaystyle\int_{-\infty}^{\infty}\int_{-\infty}^{t_1} dt_1 dt_2\, [V_I(t_1), V_I(t_2)], \\ \cdots \end{cases} \tag{10}$$

where higher orders Ω_n can be calculated in the same way. The first order is completely analytical, but the general structure can be analyzed by understanding the form of the Magnus operators. For the first order, we write the integral and perform the exchange of variables $x = z + vt$.

$$\Omega_1(\infty) = -\frac{i}{\hbar v}\int_{-\infty}^{\infty} dx \left(\boldsymbol{d}_{eg}\sigma_+ e^{\frac{i\omega_0}{v}(x-z)} + \boldsymbol{d}_{eg}^*\sigma_- e^{-\frac{i\omega_0}{v}(x-z)}\right)\cdot \boldsymbol{E}(r_\perp, 0, x). \tag{11}$$

To simplify this further, we now define the electron momentum ladder operators:

$$b = e^{-\frac{i\omega_0}{v}z},\ b^+ = e^{\frac{i\omega_0}{v}z}. \tag{12}$$

These are operators that lower (or raise) the electron momentum by $\frac{\hbar\omega_0}{v}$. In the regime where the kinetic energy of the electron is significantly larger than the energy gap of the TLS, this translates to an energy lowering (raising) operator for the electron wavefunction that changes the electron's energy by that of the TLS ($\hbar\omega_0$). With this definition in place, Ω_1 is given as

$$\Omega_1(\infty) = -\frac{i}{\hbar v}\left(b\sigma_+\boldsymbol{d}_{eg}\cdot F\{\boldsymbol{E}(r_\perp, 0, x)\}\left(\frac{\omega_0}{v}\right) + b^+\sigma_-\boldsymbol{d}_{eg}^*\cdot F^*\{\boldsymbol{E}(r_\perp, 0, x)\}\left(\frac{\omega_0}{v}\right)\right), \tag{13}$$

where F denotes the Fourier transform. The Fourier components of the electric field of a relativistic point charge have a well-known expression, and therefore, we can find Ω_1 exactly as [4]

$$\Omega_1(\infty) = -\frac{ie\omega_0}{2\pi\varepsilon_0\gamma\hbar v^2}\left(d_x K_1\left(\frac{\omega_0 r_\perp}{v\gamma}\right) + id_z K_0\left(\frac{\omega_0 r_\perp}{v\gamma}\right)\frac{1}{\gamma}\right)(b\sigma_+) -$$

$$-\frac{ie\omega_0}{2\pi\varepsilon_0\gamma\hbar v^2}\left(d_x K_1\left(\frac{\omega_0 r_\perp}{v\gamma}\right) - id_z K_0\left(\frac{\omega_0 r_\perp}{v\gamma}\right)\frac{1}{\gamma}\right)(b^+\sigma_-), \tag{14}$$

where K_m represents modified Bessel functions of the second kind and $\gamma = \frac{1}{\sqrt{1-\beta^2}}$, with $\beta = \frac{v}{c}$. To the first order in the Magnus expansion, we can write the scattering matrix as

$$S = e^{-i\left(gb\sigma_+ + g^* b^+\sigma_-\right)}, \tag{15}$$

where the interaction strength parameter g given by

$$g = \frac{e\omega_0}{2\pi\varepsilon\gamma\hbar v^2}\left(d_x K_1\left(\frac{\omega_0 r_\perp}{v\gamma}\right) + id_z K_0\left(\frac{\omega_0 r_\perp}{v\gamma}\right)\frac{1}{\gamma}\right). \tag{16}$$

An analysis of the commutation relation between the TLS ladder operators shows that the general form of the S matrix is given by

$$S = e^{-i\left(Gb\sigma_+ + G^* b^+\sigma_-\right) - iK\sigma_z}, \tag{17}$$

where G is receiving contributions from the odd orders of the Magnus expansion and K from the even orders. This can readily be seen from the commutation relations of the Pauli operators, e.g., $[\sigma_+, \sigma_-] = \sigma_z, [\sigma_z, \sigma_\pm] \propto \sigma_\pm$. This leads to the cyclical behavior in the operators Ω_n appearing in the Magnus interaction. To estimate the efficiency of using the expansion, we need to estimate integrals of the form $\frac{1}{\hbar^n n!}\int dt_1 \dots dt_n V_I^n(z + vt)$. To obtain an estimate, we look at the electric field of a point charge in the non-relativistic limit:

$$V_I \approx \frac{edr_\perp}{4\pi\varepsilon_0(r_\perp^2 + (z+vt)^2)^{\frac{3}{2}}} = \frac{ed}{4\pi\varepsilon_0 r_\perp^2}\cdot\frac{1}{\left(1 + \frac{(z+vt)^2}{r_\perp^2}\right)^{\frac{3}{2}}} = \frac{ed}{4\pi\varepsilon_0 r_\perp^2}\cdot V_I^{\text{dimensionless}}. \tag{18}$$

To make the integral dimensionless we change variables $x = \frac{z+vt}{r_\perp}$, $dt = \frac{dx}{r_\perp v}$.

$$\Omega_n \propto \frac{1}{n!}\left(\frac{ed}{4\pi\hbar v\varepsilon_0 r_\perp}\right)^n \cdot [\text{dimensionless integrals}] \approx \frac{(3\cdot 10^{-3})^n}{n!} \cdot [\text{dimensionless integrals}], \quad (19)$$

where we took $er_\perp \approx d$ and $v \approx 10^8$ m/s. We see that, in general, each order in the Magnus expansion will be three orders of magnitude smaller, which already justifies our approximation that neglects K. Furthermore, because the dimensionless integrals are oscillatory and each higher-order term oscillates faster, the discrepancy between higher-order terms in the Magnus expansion should be even larger than expected from a naïve scaling based on Eq. (19). We corroborated this argument with numerical estimates of the higher-order terms for realistic parameters.

The parameter g is a dimensionless parameter that quantifies the interaction strength. It is useful to define $g \equiv |g|e^{i\phi_g}$, where $|g|$ is the magnitude of the interaction strength and ϕ_g its phase. This coupling, as can be seen from Eq. (16), is electron-velocity-dependent. To obtain an estimate of the velocity of the free electron in order to obtain the strongest interaction possible, we consider atomic dipoles oriented along x and z. We work in the non-relativistic limit (as we will see, the strongest interaction is achieved at velocities well below the speed of light, for which $\gamma_\varepsilon \approx 1$). For a dipole along the x axis, we have

$$g = -\frac{ie\omega_0 d_x}{2\pi\varepsilon\hbar v^2} K_1\left(\frac{\omega_0 r_\perp}{v}\right) = \frac{a}{v^2} K_1\left(\frac{b}{v}\right), \quad (20)$$

$$\frac{\partial g}{\partial v} = -\frac{2a}{v^3} K_1\left(\frac{b}{v}\right) - \frac{ab}{v^4} K_1'\left(\frac{b}{v}\right) = 0 \Rightarrow -\frac{b}{v} K_1'\left(\frac{b}{v}\right) - K_1\left(\frac{b}{v}\right) = 0. \quad (21)$$

This can be evaluated numerically and results in $v_{opt} \approx \frac{b}{1.33} = \frac{r_\perp \omega_0}{1.33}$. The same analysis can be applied to a dipole pointing only along the z axis and results in $v_{opt} \approx \frac{b}{1.55} = \frac{r_\perp \omega_0}{1.55}$. Therefore, the optimal velocity depends on the spatial structure of the TLS and will be within the range

$$\frac{r_\perp \omega_0}{1.55} < v_{opt} < \frac{r_\perp \omega_0}{1.33}. \tag{22}$$

Typically, in the optical range $\hbar\omega_0$ there will be few electron volts and $r_\perp$ will be a few nanometers. We can write for simplicity $\omega_0 = a \cdot \frac{\mathrm{eV}}{\hbar}, r_\perp = b \cdot \mathrm{nm}$. It follows then that the optimal velocity of the free electron is governed by

$$a \cdot b \cdot 0.32\%\, c < v_{opt} < a \cdot b \cdot 0.38\%\, c. \tag{23}$$

For realistic parameters, the optimal velocity will always be a few percent of the speed of light, and therefore, the approximation $\gamma = 1$ is well justified.

As in the traditional PINEM analysis, it is convenient to work in the regime where the electron wavefunction is a coherent superposition of discrete energies with a small Gaussian broadening (much smaller than $\hbar\omega_0$). Thus, we may idealize the electron as a truly discrete superposition of energies evenly spaced by the TLS energy. In this notation, it is convenient to define the electron state as $|\psi_e\rangle = \sum_k C_k |E_0 + k\hbar\omega_0\rangle$. In this notation, the electron ladder operators are defined as

$$b|E\rangle = |E - \hbar\omega_0\rangle, \qquad b^+|E\rangle = |E + \hbar\omega_0\rangle. \tag{24}$$

With all these developments, both the definition of the ladder operators and the neglect of the K-terms, we may finally arrive at the main result presented in our main manuscript, in which the S-matrix is expressed as

$$S = \cos|g| - i\sin|g|\left(e^{i\phi_g} b\sigma^+ + e^{-i\phi_g} b^+\sigma^-\right). \tag{25}$$

Section IV – The evolution of the TLS before the interaction with the electron

In this section, we discuss the evolution of the state of the TLS before the interaction with the electron. As the interaction with the electron is very brief (fs time scale) as compared to typical decoherence time scales, we can consider the electron–TLS interaction as instantaneous as compared to the TLS excitation and relaxation times.

Let us suppose that a laser field or any other means of coherent manipulation acts on the atom at time $\tau = 0$. Hence, before the action of the laser field, the atom has the following density matrix on the basis $|g\rangle, |e\rangle$.

$$\rho(\tau) = \begin{pmatrix} 1 & 0 \\ 0 & 0 \end{pmatrix} (\tau < 0). \tag{26}$$

This represents the atom being in the ground state. At time $\tau = 0$, the atom interacts with a laser pulse and is excited to some state described by a density matrix ρ,

$$\rho(\tau) = \begin{pmatrix} 1-p & q \\ q^* & p \end{pmatrix} (\tau = 0). \tag{27}$$

At this point, the atom goes through relaxation and decoherence from the coupling to the environment, as described by Lindblad's master equations [5], and the resulting density matrix as a function of delay τ is given by

$$\rho(\tau) = \begin{pmatrix} 1 - pe^{-\frac{\tau}{T_1}} & qe^{i\omega_0\tau}e^{-\frac{\tau}{T_2}} \\ q^*e^{i\omega_0\tau}e^{-\frac{\tau}{T_2}} & pe^{-\frac{\tau}{T_1}} \end{pmatrix}, \tag{28}$$

where T_1 and T_2 are the longitudinal and transverse relaxation times (or as sometimes called relaxation and decoherence times) and typically $T_2 \ll T_1$; $\hbar\omega_0$ is the energy difference between the ground and the excited states of the qubit.

Section V – TLS interaction with a general electron wavefunction

In this section, we investigate the resulting EELS spectra of a general electron wavefunction after the interaction with the TLS. We consider a wavefunction composed of a superposition of energies separated by $\hbar\omega_0$. A general wavefunction for the electron can be written as a sum of wavefunctions with different central energies. We take the initial wavefunction as

$$|\psi_{in}\rangle = \sum_n C_n |E_n\rangle \otimes (a|\mathrm{g}\rangle + e^{i\phi_a} b|\mathrm{e}\rangle), \tag{29}$$

where a and b are positive real numbers satisfying $a^2 + b^2 = 1$ and $|E_n\rangle$ is defined as $|E_0 + n\hbar\omega_0\rangle$. The final wavefunction $|\psi_{out}\rangle$, is given as $|\psi_{out}\rangle = S|\psi_{in}\rangle$ so that

$$\begin{aligned} |\psi_{out}\rangle = &\sum_n C_n |E_n\rangle \otimes \left(a|\mathrm{g}\rangle + e^{i\phi_a} b|\mathrm{e}\rangle\right) \cdot \cos|g| \\ &-i \cdot \sum_n C_{n+1} |E_n\rangle \otimes \left(e^{i\phi_g} a|\mathrm{e}\rangle\right) \cdot \sin|g| \\ &-i \cdot \sum_n C_{n-1} |E_n\rangle \otimes \left(e^{i(\phi_a - \phi_g)} b|\mathrm{g}\rangle\right) \cdot \sin|g|\,. \end{aligned} \tag{30}$$

What we measure eventually in the EELS spectrum is the probability of the electron to be in a specific energy, $P_n = |\langle E_n|\psi_{out}\rangle|^2$, where

$$\begin{aligned} \langle E_n|\psi_{out}\rangle = &|\mathrm{g}\rangle \cdot \left[aC_n \cdot \cos|g| - ie^{i(\phi_a - \phi_g)} bC_{n-1} \cdot \sin|g|\right] \\ &+|\mathrm{e}\rangle \cdot \left[e^{i\phi_a} bC_n \cdot \cos|g| - ie^{i\phi_g} aC_{n+1} \cdot \sin|g|\right] \end{aligned} \tag{31}$$

and its modulus-squared is given as

$$\begin{aligned} P_n = &|C_n|^2 \cos^2|g| + |bC_{n-1}|^2 \sin^2|g| + |aC_{n+1}|^2 \sin^2|g| \\ &+2\mathrm{Re}\left\{i \cos|g| \sin|g| \left(C_n C_{n-1}^* abe^{i(\phi_g - \phi_a)} + C_n C_{n+1}^* bae^{-i(\phi_g - \phi_a)}\right)\right\}. \end{aligned} \tag{32}$$

Expressed in terms of density matrix (as defined in Eq. (27)) elements, we obtain the spectrum for a general atom (not necessarily an atom in coherent superposition):

$$P_n = |C_n|^2 \cos^2|g| + p|C_{n-1}|^2 \sin^2|g| + (1-p)|C_{n+1}|^2 \sin^2|g| \\ +2Re\{i \cos|g| \sin|g| \left(C_n C_{n-1}^* q e^{i(\phi_g)} + C_n C_{n+1}^* q^* e^{-i(\phi_g)}\right)\}. \quad (33)$$

Calculating the average energy gain for the initially symmetric electron ($|C_n| = |C_{-n}|$):

$$\langle E_{gain} \rangle = \hbar\omega_0 \sin^2|g| \,(2p-1) + i\,\hbar\omega_0 \cos|g| \sin|g| \left(q e^{i(\phi_g)} \sum C_n C_{n-1}^* - q^* e^{-i(\phi_g)} \sum C_n C_{n+1}^*\right). \quad (34)$$

The expression $\sum C_n C_{n-1}^*$ is the expectation value of the ladder operator b. Approximating for small g, it is convenient to write

$$\langle E_{gain} \rangle = \hbar\omega_0 |g|^2 (2p-1) + i\hbar\omega_0 |g| \left(q e^{i(\phi_g)} \langle b \rangle - q^* e^{-i(\phi_g)} \langle b^+ \rangle\right). \quad (35)$$

The second term comes from the interference between the different electron energies (as it contains the off-diagonal elements of the density matrix). This term decays as the system goes through decoherence. For example, we can look at time τ for which $\tau \ll T_1$ and assume that $T_2 \ll T_1$, and then, the decoherence will be expressed as a decay of the interference term:

$$P_n(\tau) = |C_n|^2 \cos^2|g| + |bC_{n-1}|^2 \sin^2|g| + |aC_{n+1}|^2 \sin^2|g| \\ +2Re\{i \cos|g| \sin|g| \left(C_n C_{n-1}^* a b^* e^{i\phi} + C_n C_{n+1}^* b a^* e^{-i\phi}\right)\} e^{-\frac{\tau}{T_2}}. \quad (36)$$

We consider two simple configurations of electron states. First, we consider an unshaped electron, for which $C_n = \delta_{n,0}$. This corresponds to the case in many standard EELS and CL microscopy experiments. The electron can either gain/lose energy because of the interaction with the TLS or remain unchanged:

$$P_{-1} = (1-b^2) \sin^2|g|, P_0 = \cos^2|g|, P_1 = b^2 \sin^2|g|\,. \quad (37)$$

From the EELS spectrum, we can conduct the population statistic of the qubit. This term has contributions only from incoherent terms, as the electron cannot undergo interference with itself, and therefore, when the system goes through relaxation the solution will be

$$P_{-1} = \left(1 - b^2 e^{-\frac{\tau}{T_1}}\right) \sin^2|g|, P_0 = \cos^2|g|, P_1 = b^2 \sin^2|g| e^{-\frac{\tau}{T_1}}. \quad (38)$$

By repeatedly measuring the interaction in this way, we can obtain the EELS spectrum for different time delays τ and extract information, such as the energy gaps and lifetimes of atoms. However, this includes no information about the coherent structure of the probed system. This measurement scheme is presented in the main text's Fig. 2. To observe coherent properties, we need to use an electron with multiple energy levels distanced from each other by the energy gap of the atomic system. The different energies of the electron interfere during the interaction and create observable changes in the EELS spectrum. The simplest case to check is an electron with two energies distanced by $\hbar\omega_0$ with a defined phase between them. Such an electron can be created approximately by using a PINEM interaction. It should be noted that it is not necessary to use exactly the electron that has specifically two energies. To observe quantum interference, the only requirement is that the electron has at least two energies distanced by the energy of the qubit transition $\hbar\omega_0$. However, the simplest and most elegant way to demonstrate the concept is to use a bi-energetic electron.

The wavefunction of such an electron can be written as

$$|\psi_e\rangle = \frac{1}{\sqrt{2}}\left(\left|E_0 - \frac{1}{2}\hbar\omega_0\right\rangle + e^{i\phi_e}\left|E_0 + \frac{1}{2}\hbar\omega_0\right\rangle\right). \quad (39)$$

The resulting EELS spectra will contain four peaks:

$$\begin{cases} P_{-\frac{1}{2}} = \frac{1}{2}\cos^2|g| + \frac{1}{2}a^2\sin^2|g| - \cos|g|\sin|g|\,ab\cdot\sin\left(\phi_a - \phi_e - \phi_g\right) \\ P_{\frac{1}{2}} = \frac{1}{2}\cos^2|g| + \frac{1}{2}|b|^2\sin^2|g| + \cos|g|\sin|g|\,ab\cdot\sin\left(\phi_a - \phi_e - \phi_g\right) \\ P_{-\frac{3}{2}} = \frac{a^2}{2}\sin^2|g| \\ P_{\frac{3}{2}} = \frac{b^2}{2}\sin^2|g| \end{cases}, \tag{40}$$

Since the coupling is typically weak, we can approximate and obtain

$$\begin{cases} P_{-} = \frac{1}{2} - |g||ab|\sin\left(\phi_a - \phi_e - \phi_g\right) \\ P_{+} = \frac{1}{2} + |g||ab|\sin\left(\phi_a - \phi_e - \phi_g\right) \end{cases}. \tag{41}$$

This is an interesting expression, as the phase ϕ_e is controlled by the shaped electron, the phase ϕ_g depends on the internal structure of the TLS, such as the size of the dipole in each direction, and the phase ϕ_a depends on the coherent superposition of the TLS. Thus, we can set a precise phase for the electron wavefunction to measure the phase difference of the TLS states. Alternatively, we can measure the relative size of the different dipole components d_x and d_z by measuring ϕ_g. Another notable property of this expression is that the contrast in the resulting EELS signal is proportional to $|g|$, as opposed to $|g|^2$.

The value $|ab|$ corresponds to the size of the off-diagonal elements of the density matrix in the general case. These terms typically decay exponentially with the characteristic time T_2. We propose a possible scheme to measure T_2: A qubit is prepared in an initial superposition $|\psi\rangle = \frac{1}{\sqrt{2}}\left(|e\rangle + e^{i\phi_a}|g\rangle\right)$, then go through decoherence for a duration τ, before being probed by a bi-energetic electron. We then measure the change in the EELS peaks (which is proportional to $|g|$) and extract T_2 by repeating this measurement for different time delays, according to the formula:

$$\Delta P = P_+ - P_- = e^{-\frac{\tau}{T_2}}|g|\sin\left(\phi_a - \phi_e - \phi_g\right). \tag{42}$$

We would also like to exploit this direct dependence on $|g|$ to measure the relaxation time T_1. For this, we discuss a simplified case that assumes $T_1 \gg T_2$ (a more general scenario can be solved by extending the same approach). In this case, the density matrix of the atom shortly after the excitation is well approximated by $\rho(\tau) = \begin{pmatrix} 1 - |a_2|^2 e^{-\frac{\tau}{T_1}} & 0 \\ 0 & |a_2|^2 e^{-\frac{\tau}{T_1}} \end{pmatrix}$. On this qubit, we can perform a $\pi/2$ pulse before the interaction with the electron using another laser pulse, which corresponds to the rotation of the qubit's state around the x-axis in the Bloch sphere by 90 degrees. As this corresponds to applying a unitary transformation on the qubit's state $U = \frac{1}{\sqrt{2}}\begin{pmatrix} 1 & -i \\ -i & 1 \end{pmatrix}$, the resulting density matrix of the qubit after this operation is given by:

$$\rho_{\frac{\pi}{2}}(\tau) = U\rho(\tau)U^+ = \begin{pmatrix} \frac{1}{2} & i\left(\frac{1}{2} - |a_2|^2 e^{-\frac{\tau}{T_1}}\right) \\ -i\left(\frac{1}{2} - |a_2|^2 e^{-\frac{\tau}{T_1}}\right) & \frac{1}{2} \end{pmatrix}. \tag{43}$$

The size of the off-diagonal element is now $\frac{1}{2} - |a_2|^2 e^{-\frac{\tau}{T_1}}$, and so the interaction with bi-energetic electron will result in changes of the EELS peaks proportional to $|g|$ which decay with the factor of T_1, and so T_1 can be extracted with relatively lower EELS resolution:

$$\Delta P = P_+ - |g|\left(1 - 2|a_2|^2 e^{-\frac{\tau}{T_1}}\right)\sin\left(\frac{\pi}{2} - \phi_e - \phi_g\right). \tag{44}$$

The above results all discuss how the electron qubit interaction can be used in order to extract information about the qubit, but Eq. (35) shows that, in general, we can obtain an electron energy gain and loss that is proportional to $|g|$ rather than to $|g|^2$ when $\langle b \rangle \neq 0$, presenting how the reliance on quantum interference is used here not only to extract information about the coherent

phases of the TLS but also to intensify the energy transfer between the electron and the TLS. This kind of enhanced interaction will lead eventually to an enhanced CL signal, as the electron transfers this energy to the excitation of the TLS, which will eventually result in a stronger emission of radiation. It should be noted that a PINEM-generated electron without free space propagation or other amplitude manipulation will not have an energy gain/loss proportional to $|g|$. To show this, we recall the wavefunction of a PINEM modulated electron [6] with a laser frequency equal to $\omega = \omega_0/l$:

$$|\psi_e\rangle = \sum_n e^{i\phi n} J_n(2|g^{PINEM}|)|E_0 + \hbar n\omega\rangle\,. \tag{45}$$

The expectation value of the b operator will always be zero according to the Bessel functions identity:

$$\sum_n J_n(x)J_{n-l}(x) = 0\,. \tag{46}$$

Nevertheless, the EELS signal still contains features proportional to $|g|$, such as the height difference between EELS peaks. For the average gain to change, or to obtain an enhancement of the energy transfer, the initial electron must be shaped by amplitude modulation, not only by phase modulation. This can be achieved by having a distance of free space propagation after a PINEM interaction. The PINEM induces only phase modulation, but then the electron dispersion in free space transforms the phase modulation into amplitude modulations. Similar enhancements, based on the modulation of free electrons, were proposed for the first time using a semiclassical analysis in [4]. We show how our quantum description of the interaction conforms to part of the results of the semiclassical theory [4] and also generalizes related work on the quantum klystron [7]. The semiclassical formalism used in these papers can describe the enhancement of the interaction with

qubits due to the phase modulation of the electrons but cannot describe the resulting EELS spectrum as it relies on quantum interference, which is crucial for quantum measurements. Another technique for enhancing the CL due to the interaction with free electrons is described in Section VI.

The most attractive quantum systems for a proof of concept are those with large transition dipole moments, such as perovskite nanocrystals. According to Eq. (16), we can estimate the interaction strength for perovskites. We consider a typical transition dipole moment of $d \approx 288$ D, excited state energy $\hbar\omega_0 \approx 3$eV, electron speed chosen to be optimal according to Eq. (22) is equal to ~7% the speed of light (1.25 keV), and distance from the qubit $r_\perp = 6$ nm. Notice that the even for relatively such slow electron, the energy of the electron is much larger than the energy of the qubit and the paraxial approximation is expected to hold. For these parameters, the interaction strength is approximately $|g| \approx 0.1$. The typical dipole of the molecules is usually considerably smaller. For example, the dipole moment of a water molecule is $d \approx 2.0\ D$. In this case, the interaction constant equals $|g| \approx 0.7 \cdot 10^{-3}$. The resulting coupling parameter $|g| \approx 0.1$, can be readily detected in typical EELS detectors. Such interaction conditions enable a temporal resolution of about a hundred femtoseconds and a spatial resolution reaching 1.4 nm at these electron energies [8].

The standard deviation of the EELS features after N measurements can be estimated as $\frac{1}{\sqrt{N}}$. This means that the relative error in the interference measurements (where the measured result is $\sim|g|$) approximately equals $\frac{1}{g\sqrt{N}} \cdot 100\%$. To achieve a standard deviation of 1% of the result, in the case of the strongest interaction of $|g| = 0.1$ we need approximately 10^6 repetitions, i.e., one million electrons, with current laser repetition rates, this implies an integration time of ~1 s. Note

that standard EELS systems and current PINEM experiments are performed at higher velocities (e.g., 80 keV electrons show an optimal coupling parameter $|g| = 0.025$, well within current detection capabilities). Nevertheless, highly sensitive EELS also exist at low acceleration voltages. [9]

Section VI – Observation of qubits emitting radiation superradiantly

In this section, we consider the weak interaction ($|g| \ll 1$) of a free electron with a group of N non-interacting qubits close to each other and consider how their superradiant behavior can be observed through the EELS signal. In this case, the scattering matrix S will have the form

$$S = \prod_i S_i = \prod_i e^{-i\left(g\sigma_+^i b + g^*\sigma_-^i b^+\right)}, \tag{47}$$

where $\sigma_\pm^i$ are Pauli matrices for the i^{th} qubit. If the qubits are prepared in the collective state $|\psi_A\rangle$ and they interact with a monoenergetic electron $|E_0\rangle$, in the case of weak interaction strength ($|g| \ll 1$) we can approximate the resulting final state $|\Psi_\mathrm{f}\rangle$ to second order in $|g|$:

$$|\Psi_\mathrm{f}\rangle = S|E_0\rangle|\psi_A\rangle \approx$$

$$\approx (1 - N|g|^2)|E_0\rangle|\psi_A\rangle - i\left[\sum_i g\sigma_+^i\,|E_0 - \hbar\omega_0\rangle|\psi_A\rangle + \sum_i g^*\sigma_-^i\,|E_0 + \hbar\omega_0\rangle|\psi_A\rangle\right]. \tag{48}$$

Then, the resulting spectrum has the form

$$\begin{cases} P_0 = 1 - N|g|^2 \\ P_+ = |g^2| \sum_i \langle \psi_A | \sigma_-^i | \psi_A \rangle = |g|^2 \cdot \left(\frac{2\langle E_{qubits} \rangle}{\hbar\omega_0} + \frac{N}{2} \right) \\ P_- = |g^2| \sum_i \langle \psi_A | \sigma_+^i | \psi_A \rangle = -|g|^2 \cdot \left(\frac{2\langle E_{qubits} \rangle}{\hbar\omega_0} - \frac{N}{2} \right) \end{cases}, \quad (49)$$

where P_0 is the probability that the energy of the electron will not be changed, P_+ is the probability that an electron's energy will increase on $\hbar\omega_0$, and P_- is the probability that an electron's energy will decrease on $\hbar\omega_0$. Then, the average energy gain equals

$$\langle E_{\text{gain}}(\tau) \rangle = \hbar\omega_0(\Delta P) = \hbar\omega_0 |g|^2 \frac{4\langle E_{\text{qubits}} \rangle}{\hbar\omega_0}, \quad (50)$$

where $\langle E_{\text{qubits}} \rangle$ is the average energy of the superradiant qubits. The intensity of superradiant emission is connected with $\langle E_{\text{qubits}} \rangle$ [10]:

$$I_{\text{superradiant}}(\tau) = -\frac{d\langle E_{\text{qubits}}(\tau) \rangle}{dt}. \quad (51)$$

Hence, by measuring the gain for different time delays and using Eq. (52), we can reconstruct the superradiant emission of the qubits.

Eq. (50) shows that the electron states with energy gain/loss are entangled with qubit states raised *symmetrically*. This informs us that, even if we did not pre-excite the qubits as suggested in the measurement scheme, the interaction with the electron results in an (at least partly) symmetric state. Such a state, as we know, given that the qubit–qubit interactions are sufficiently weak and the qubits are sufficiently close, will emit superradiantly [10]. This type of superradiant emission is a form of coherent enhancing of the CL signal.

Section VII – Extracting the local density of photonic states (LDOS)

In this section, we discuss how LDOS can be extracted from the interaction with free electrons. In the case of qubits with weak non-radiative relaxation, T_1 is directly related to the qubit's spontaneous emission rate $\gamma = 1/T_1$ and is influenced by its optical environment – the local density of optical states (LDOS). An emitter at a location $\boldsymbol{r}_0$ and oriented along direction z has [9]

$$\gamma = \frac{\omega_0}{\hbar\varepsilon_0}|\boldsymbol{d}|^2\rho_z(\boldsymbol{r}_0,\omega_0) = \frac{4\omega_0^2}{\pi\hbar\varepsilon_0 c^2}|\boldsymbol{d}|^2\mathrm{Im}\{G_{zz}(\boldsymbol{r}_0,\boldsymbol{r}_0,\omega)\}, \tag{52}$$

where $G_{zz}(\boldsymbol{r}_0,\boldsymbol{r}_0,\omega)$ is the zz component of the Green function and $\rho_z(\boldsymbol{r}_0,\omega_0)$ is the LDOS. Typically, γ is measured by optically exciting a group of emitters in an area and measuring the resulting emission as a function of time [11]. Indirect measurement is through the spectrum [11], where the broadening of the peak depends on the lifetime (competing with other processes of incoherent broadening). These techniques are limited by their spatial resolution due to the optical wavelength and often require many emitters to collect sufficient signal.

Advances in CL enable measurement of the LDOS with deep sub-wavelength resolution using an electron probe. More recent advances use time-resolved CL to achieve a direct measurement of T_1 at such deep-subwavelength resolutions [12, 13]. The use of shaped-electron–qubit interactions poses an alternative means of measuring the LDOS. Its relative advantage is the femtosecond time resolution that arises from the durations of the electron pulses and laser pulses in our scheme.

Section VIII – Measurement of a qubit state

In this section, we discuss further the scheme proposed in Section III in the main text for measuring the complete qubit state on the Bloch sphere using coherently shaped free electrons. Eq. (44) provides the resulting EELS spectrum of a bi-energetic electron interacting with a qubit in general coherent superposition. The height difference between the two main peaks is given by

$$\Delta P = (P_+ + P_-)|g| \sin(\theta_a) \sin(\Phi)\,, \tag{53}$$

where $\Phi = \phi_a - \phi_e - \phi_g$ and θ_a, ϕ_a are the angles describing the qubit location on the Bloch sphere (Fig. 3 in the main text). By scanning on different electron phases, one can find the phase ϕ_e for which ΔP is maximal; in this phase, the condition $\sin(\Phi) = 1$ is achieved and ϕ_a is extracted. Then, by measuring ΔP we conclude $|g| \sin(\theta_a)$. This method, however, gives an inconclusive answer to the question about the qubit state, as the function $\sin(\theta_a)$ leaves an ambiguity concerning whether the qubit is in the upper or lower half of the Bloch sphere. To solve this, one needs to look at the other side lobes in the EELS spectrum, which correspond to the energies $E_+ + \hbar\omega_0$ (gain lobe) and $E_- - \hbar\omega_0$ (loss lobe), as they are not affected by quantum interference. If the gain lobe is higher, then the qubit was in the lower half of the Bloch sphere (meaning that without quantum interference, it will mostly "give" energy to the electron) and otherwise in the upper half. The drawback of this method is that the height of the side lobes is proportional to $|g|^2$, increasing the required sensitivity of the EELS measurement or, alternatively, increasing the number of repetitions required to obtain a measurement. A possible means of bypassing this drawback is to "flip" the qubit 90 degrees around the *x*-axis using conventional coherent control methods (for example, by performing an additional $\pi/2$ pulse before the interaction with the electron) and then measure again using the same method, by combining the

measurement result from the two measurements we can conclude the exact location on the Bloch sphere as illustrated in Fig. 3. This technique uses only measurements of probability differences proportional to $|g|$, however, it requires an additional laser pulse, increasing the measurement's complexity.

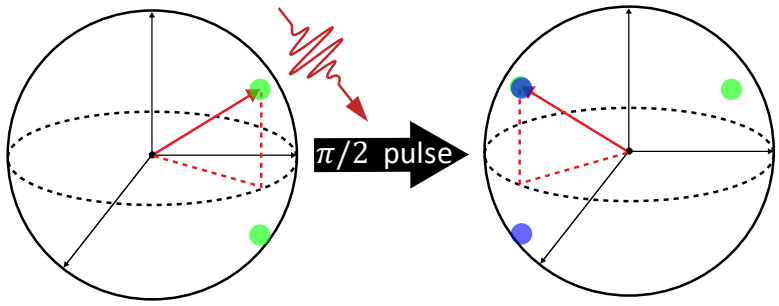

Fig. 3. Determining the exact location on the Bloch sphere using an additional $\pi/2$ pulse. The first measurement leaves ambiguity about the qubit's location on the Bloch sphere; the green circles represent the two options we cannot distinguish between them. After performing an additional $\pi/2$ pulse and measuring again, we yet again get two options that we cannot distinguish between (blue circles), but by matching the two measurements, we conclude the full state of the qubit.

Section IX – The S matrix formalism

In this section, we discuss the S matrix formalism and how it can be exploited to calculate more complicated interactions. In the previous sections, we derived the scattering matrix for the interaction of a free electron and a qubit. The most general expression takes the form:

$$S_{qubit} = e^{-i\left(Gb\sigma_+ + G^* b^+ \sigma_- \right) - iK\sigma_z}. \tag{54}$$

Analysis of the interaction between free electrons and quantized light fields gives a similar scattering matrix as shown in [14],

$$S_{PINEM} = e^{-i\left(gba^+ + g^* b^+ a\right)}, \tag{55}$$

The resemblance is not surprising, as we can conclude from the Magnus expansion or other perturbative expressions that in the most general case the scattering matrix should be given as exponentiation of the sum of the relevant creation and annihilation operators (in an energy-conserving manner) and their commutation relations. One of the advantages of presenting the interaction in a scattering matrix form is the ability to calculate the interaction of a single electron wavefunction with multiple non-interacting systems by composing (see Fig. 4) the scattering matrices. Since the subsystems are non-interacting and the electron ladder operators are commuting, the exponent in the final scattering matrix is the sum of the exponents of the scattering matrices. This approach can be used to calculate the interaction of the electron with multiple qubits (as done in Section VI) or calculate more exotic interactions such as chain of consecutive PINEM and qubit interactions. Other types of interactions can also be calculated using a similar formalism (Fig. 4).

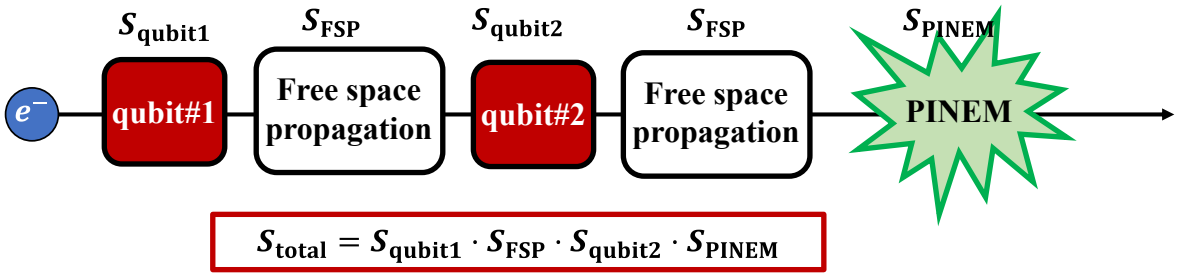

Fig. 4. Calculating chain of interactions. The electron goes through a mixture of different interactions such as qubit-electron and PINEM interactions. Every interaction is described by a scattering matrix S. To calculate the final state of the electron, we need to compose the scattering matrices.

Section X – Comparison to typical EELS theory

In this section, we present the conceptual differences between the standard EELS theory and our model. Specifically, we show that the standard EELS theory coincides with our model when a quantum two-level system is initially in the ground state. However, when the quantum two-level system is initially in the coherent superposition state, the standard EELS theory cannot provide the correct prediction. The deviation arises from the fact that in standard EELS, the energy loss is formulated in terms of the susceptibility of the target, which is calculated assuming the target is initially in its ground state. Therefore, our results can be seen as a version of the EELS theory in which the target is initially in a non-equilibrium, time-varying state. This difference is of course not small, leading to energy-gain and interference effects which enable the scheme and ideas presented in our work.

Typically, in EELS theory, the energy loss of the electron interacting with the system depends on the system's multipolar polarizability (or alternatively susceptibility), which describes the system's response to the external field. For example, for a spherically symmetric system, the energy loss can be expressed as [15]:

$$\Gamma(\omega) = \frac{4\alpha c}{\pi v^2} \sum_{l=1}^{\infty} \sum_{m=-l}^{l} \frac{\left(\frac{\omega}{v}\right)^{2l}}{(l+m)!\,(l-m)!} K_m^2\left(\frac{\omega r_\perp}{v}\right) Im\{\alpha_l(\omega)\}, \tag{56}$$

where:

$$Im\{\alpha_l(\omega)\} = \alpha^{2l+1} \frac{l\varepsilon(\omega) - 1}{l\varepsilon(\omega) + l + 1}, \tag{57}$$

which is the sphere's non-retarded multipolar polarizability of order l.

Consider a quantum two-level system in a general state described by a density matrix with non-zero off-diagonal elements:

$$\rho_a = \begin{pmatrix} 1-p & qe^{i\omega_0 t} \\ q^* e^{-i\omega_0 t} & p \end{pmatrix}. \tag{58}$$

The dipole polarization of the system in the case of non-zero off-diagonal elements exist even without an external electric field (thus acting on the electron analogously to an external AC field):

$$\boldsymbol{d}(\boldsymbol{t}) = Tr\left[\rho_a \boldsymbol{d_{eg}}\right] = Tr[\rho_a \sigma_+]\boldsymbol{d} = 2Re\left[qe^{i\omega_0 t}\right]\boldsymbol{d}. \tag{59}$$

Hence, the system cannot be fully described by the polarizability because the dipole moment of the TLS has an imposed initial time variation, which is not purely induced by the electron, as would be the case in the standard EELS theory. Such imposed initial time variation maps to the off-diagonal elements of the initial TLS density matrix. In our paper, those off-diagonal elements can change the interaction substantially by using shaped electrons. The way for how to measure such elements is one of the key suggestions in our paper.

In the case where the TLS is initially in the ground state, so that its dipole moment is purely induced by the electron, our results are in correspondence with the standard EELS theory. In particular, let us show that our formalism reproduces Eq. (56) in the absence of initial quantum coherence in the TLS. To see that, we consider only the first order of the multipolar expansion, $l = 1$, since we are interested in dipole interactions, and $\alpha_1(\omega)$ should coincide with the polarizability of a point particle in the case of $d_x = d_y = d_z = d$ [11]:

$$\alpha_{ij}(\omega) = \delta_{ij}\frac{d^2}{\hbar}\left[\frac{1}{(\omega_0 - \omega) - \frac{i\gamma}{2}} + \frac{1}{(\omega_0 + \omega) + \frac{i\gamma}{2}}\right]. \tag{60}$$

For positive frequencies (related to energy loss), Eq. (56) reduces to:

$$\Gamma(\omega) = \frac{4\alpha c}{\pi v^2} \cdot \frac{\omega^2 d^2}{\hbar v^2} \cdot \frac{\frac{\gamma}{2}}{(\omega_0 - \omega)^2 + \frac{\gamma^2}{4}} \left[K_0^2 \left(\frac{\omega r_\perp}{v} \right) + K_1^2 \left(\frac{\omega r_\perp}{v} \right) \right]. \tag{61}$$

We see that the energy loss has resonance in the two-level system transition frequency $\omega = \omega_0$, and is broadened by the finite lifetime of the excited state. Our formalism does not capture this broadening since we treat the two-level system in a more idealistic manner (this broadening will typically be undetectable in the EELS interaction because of the incoherent energy width of the initial electron, also called the zero-loss peak width).

Now to find the probability of energy loss, we integrate over the frequencies assuming that the resonance is sharp enough so the Bessel's function can be taken out of the integral:

$$P_{EELS} = \int d\omega \Gamma(\omega) \approx \frac{4\alpha c \omega_0^2 d^2}{\hbar v^4} \left[K_0^2 \left(\frac{\omega_0 r_\perp}{v} \right) + K_1^2 \left(\frac{\omega_0 r_\perp}{v} \right) \right]. \tag{62}$$

In our case, this probability in the case where $d_z = d_\perp = d$, is given according to Eqs. (16) and (25) (modified to cgs units, in the non-relativistic case $\gamma = 1$), we can see that:

$$P = \sin^2(|g|) \approx |g|^2 = \frac{4\alpha c \omega_0^2 d^2}{\hbar v^4} \left[K_0^2 \left(\frac{\omega_0 r_\perp}{v} \right) + K_1^2 \left(\frac{\omega_0 r_\perp}{v} \right) \right] = P_{EELS}. \tag{63}$$

To conclude this section, we found a direct correspondence between our theory and the standard EELS approach in the case when the system is incoherent (in the. Sense of zero off-diagonal density matrix elements) and in the limiting case of weak interaction ($|g| \ll 1$).

Regarding the strength of the interaction, it is worth noting that for systems with larger g (as discussed in the main text), our approach goes beyond the first-order perturbative approach of

the electron-material interaction. In this case, our approach generalized beyond Eq. (63) even in the ground state limit.

References

[1] D. B. Williams, C. B Carter, *Transmission Electron Microscopy* (Springer, Boston, 2009).

[2] M. E. Peskin and D. V. Schroeder, "*An Introduction to Quantum Field Theory"* (CRC Press, Reading, USA, 2018).

[3] W. Magnus, On the exponential solution of differential equations for a linear operator, *Comm. Pure Appl. Math.* **7**(4), 649-673, (1954).

[4] A. Gover and A. Yariv, Free-electron−bound-electron resonant interaction, *Phys. Rev. Lett.* **124**, 064801 (2020).

[5] H.-P. Breuer, *The theory of open quantum systems* (Oxford University Press, New York 2002).

[6] A. Feist et al. "Quantum coherent optical phase modulation in an ultrafast transmission electron microscope." *Nature* **521**, 200 (2015).

[7] D. Ratzel et al., A quantum klystron – controlling quantum systems with modulated electron beams, arXiv:2004.10168

[8] D. C. Bell, and N. Erdman, *Low Voltage Electron Microscopy: Principles and Applications,* (Chichester, UK, 2012).

[9] G. Bracco, and B. Holst, *Surface Science Techniques*, (Springer, Berlin, 2013).

[10] M. Gross, and S. Haroche. "Superradiance: an essay on the theory of collective spontaneous emission" *Physics Reports* **93**, 301 (1982).

[11] L. Novotny, *Principles of Nano-Optics* (Cambridge University Press, New York, USA 2012).

[12] A. Polman et al., "Electron-beam spectroscopy for nanophotonics", *Nat. Materials* **18**, 1158-1171 (2019).

[13] M. Kociak, "Cathodoluminescence in the scanning transmission electron microscope", *Ultramicroscopy* **176**, 112 (2017).

[14] O. Kfir, Entanglements of Electrons and Cavity Photons in the Strong-Coupling Regime. *Phys. Rev. Lett.* **123**, 103602 (2019).

[15] F. J. G. Abajo, Optical excitations in electron microscopy, *Rev. Mod. Phys.* **82**, 209 (2010).